Proc. Natl. Acad. Sci. USA
Vol. 87, pp. 9343–9347, December 1990
Biophysics

Thickness determination of biological samples with a *z*-calibrated scanning tunneling microscope

(purple membrane/bacterial surface protein/monolayer techniques/crystalline gold)

ZHOUHANG WANG*, THOMAS HARTMANN, WOLFGANG BAUMEISTER, AND REINHARD GUCKENBERGER†

Max-Planck-Institut für Biochemie, Abteilung Molekulare Strukturbiologie, D-8033 Martinsried, Federal Republic of Germany

Communicated by C. F. Quate, August 13, 1990

ABSTRACT **A single-tube scanning tunneling microscope has been *z*-calibrated by using atomic steps of crystalline gold and was used for measuring the thickness of two biological samples, metal-coated as well as uncoated. The hexagonal surface layer of the bacterium *Deinococcus radiodurans* with an open network-type structure shows thickness values that are strongly influenced by the substrate and the preparation method. In contrast, the thickness of the purple membrane of *Halobacterium halobium* with its densely packed less-corrugated structure exhibits very little variation in thickness in coated preparations and the values obtained are in good agreement with x-ray data.**

Transmission electron microscopy is a very powerful technique for determining the size and shape of biological macromolecules. Technical advances have made it possible to attain subnanometer resolution with various two-dimensional periodic arrays (e.g., refs. 1–5). Any transmission electron micrograph, however, is basically a two-dimensional projection of a three-dimensional object. *z*-axis information about the specimen, in particular its thickness, is only obtained by indirect means [e.g., shadow-length measurements of samples coated with metal films at an oblique angle (6) or thin sectioning of positively or negatively stained material (7)]. The accuracy of these measurements is not better than 2–4 nm. Tomographic techniques (i.e., combining the information from tilt series) retrieve the three-dimensional structure and, therefore, the thickness of the specimen with higher accuracy but at the expense of considerable experimental effort. Due to the incompleteness of data caused by the restricted range of tilt angles, resolution is usually anisotropic; the *z* resolution may be considerably lower than the lateral resolution.

In contrast, the scanning tunneling microscope (STM) provides direct thickness information: the STM monitors the *z* position of the tunneling tip, which follows the surface profile of the sample when scanning in the constant current mode. At the same time the STM allows the experimenter to apply a wide range of experimental conditions, including ambient pressure and aqueous environments. Therefore, in spite of the limited lateral resolution so far achieved with biological samples, high-precision thickness measurements by STM represent valuable complementary information to transmission electron microscope (TEM) data. Such data may also be used to constrain the three-dimensional reconstructions from TEM data, thus improving their *z* resolution.

In this communication we describe methods for *z* calibration of STMs, which is a prerequisite for accurate thickness measurements, and we apply the technique to two types of biological specimens. The first is the purple membrane from *Halobacterium halobium*, a membrane crystal containing one protein species, bacteriorhodopsin (8, 9). The highly ordered hexagonal lattice (plane group *p*3) has a lattice constant of 6.3 nm. The purple membrane is a very compact structure; the membrane thickness is ≈4.7 nm, with a surface corrugation of <0.7 nm (10). Patches of purple membrane are typically 0.5–1 μm in diameter.

The second specimen is an eubacterial surface protein, the hexagonally packed intermediate (HPI) layer, from the bacterium *Deinococcus radiodurans*. The HPI layer (plane group *p*6) has a lattice constant of 18 nm and is composed of hexamers of a single polypeptide with a molecular mass of 105 kDa (11). In contrast to purple membrane, the HPI layer is a highly corrugated network-type structure. No accurate thickness measurements are available for this structure so far; based on a variety of techniques, the thickness has been estimated to be in the range of 6.9–8.6 nm (6). We have used different supports and specimen preparation techniques to evaluate the reliability and the accuracy of our STM thickness measurements.

MATERIALS AND METHODS

STM Setup. Most of the experiments described in this communication were performed with an STM of the Besocke-type (12) described in detail elsewhere (13). This STM uses a tube scanner and operates at ambient pressure. A special preamplifier allows STM images to be obtained at tunneling currents (I_t) as low as 0.1 pA. For comparison, some of the measurements on gold were done also in air with a typical "pocket-size" STM with a tripod scanner, which is used routinely for high-resolution work.

Preparation of a Gold Standard for *z* Calibration of the STM. For *z* calibration of our STM single-tube scanner, we used the monoatomic steps of the (100) surface of crystalline gold. Crystalline gold has a face-centered cubic structure with a lattice constant of $a = 0.408$ nm. Since one atom is situated in the middle of each cube face, the (100) surface (which is composed of such faces) has a square lattice structure with an effective lattice constant of $a/\sqrt{2} = 0.288$ nm. The height of a monoatomic step is $a/2 = 0.204$ nm.

One may use one of several more or less tedious procedures for producing clean atomically flat gold surfaces (e.g., refs. 14–16). We used the following simplified procedure: A pure gold foil (purchased from a local jewelry company) with a thickness of 0.1 mm was chemically cleaned with 30% (vol/vol) HNO_3. At this stage the gold foil shows substantial corrugation in STM images and no indications of regular surface structure. For annealing, the foil, held by a "tweezer" made of tungsten wire, is heated with a Bunsen flame to

The publication costs of this article were defrayed in part by page charge payment. This article must therefore be hereby marked "*advertisement*" in accordance with 18 U.S.C. §1734 solely to indicate this fact.

Abbreviations: STM, scanning tunneling microscope; HPI, hexagonally packed intermediate; TEM, transmission electron microscope; U_{tip}, voltage at the tip; I_t, tunneling current.

*Present address: Department of Chemistry, Lash Miller Chemistry Laboratory, University of Toronto, Toronto, ON M5S 1A1, Canada.
†To whom reprint requests should be addressed.

a temperature near the melting point of gold (1336 K). The color of the foil changes from gold to reddish yellow during heating. After cooling in air the gold foil shows regular structures with large terraces that are rectangular in shape (Fig. 1). In some areas small terraces of a triangular shape can be observed that are inclined with respect to the rectangular terraces.

Purple Membrane Preparation Obtained by Spreading at an Air–Water Interface. Purple membranes were prepared as described (17). To obtain even coverage of the specimen supports with purple membrane sheets, we spread them at an air–water interface. The technique we used is reminiscent of a procedure first described by Trurnit (18) for spreading monomeric and oligomeric soluble proteins. A Langmuir trough was filled with distilled water and the initial area was set to 200 cm^2. A glass rod (3 mm in diameter) was placed vertically in the trough extending ≈20 mm above the water level. A suspension of purple membranes was mixed with water and glycerol to a final concentration of 60 μg/ml in 60% (vol/vol) glycerol. This suspension (400 μl) was applied to the hemispherical top of the glass rod at a constant flow rate of 100 μl/min. The liquid, flowing down along the glass rod as a thin film, spreads when reaching the water surface. The spreading is driven by the difference in surface tension between pure water and 60% glycerol of 3 mN/m (19), where the glycerol solution has the lower surface tension. The glass rod helps the spreading compete against the unfavorable density difference; when applied as droplets, most of the suspension "drowns" because the density of 60% glycerol is 13% higher than that of pure water. The glycerol becomes diluted in the aqueous subphase, and the purple membrane remains at the air–water interface, as indicated by lateral pressure/area recordings made while decreasing the surface area (Fig. 2 *Upper*). The purple membrane at the interface was then transferred to solid supports: electron microscope grids coated with carbon (C) for TEM and coverslips or small mica pieces coated with C or platinum/carbon (Pt/C) for STM. For transfer, the layer at the interface was compressed to a lateral pressure of 20 mN/m. The solid supports were placed onto the surface face down, as described by Langmuir and Schaefer (20). They were allowed to rest there for 2 min

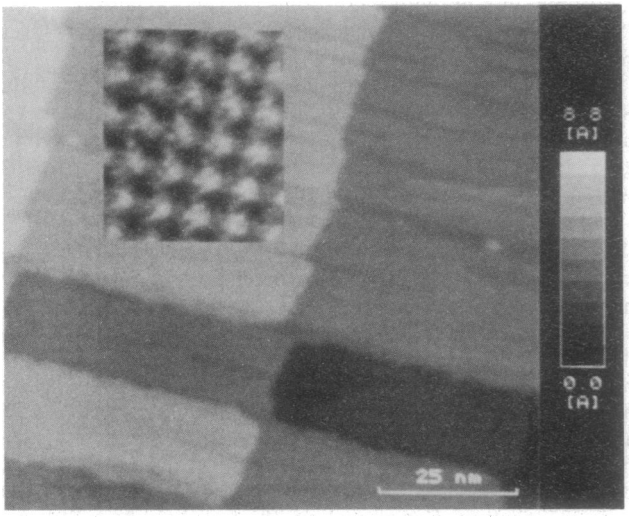

FIG. 1. STM picture of the gold (100) surface after annealing, showing monosteps and large terraces. The image was processed to remove the ramp and the distortion caused by thermal drift. Tunneling parameters: voltage at the tip (U_{tip}) = −10 mV; I_t = 1.0 nA. (*Inset*) Atomic resolution picture of this surface at much higher magnification; the image was taken in constant current mode as all images presented here and processed by Fourier filtration. Atomic corrugation is ≈0.03 nm; the lattice constant is 0.288 nm. Size = 1.3 nm × 1.6 nm. Tunneling parameters: U_{tip} = −5 mV; I_t = 100 nA.

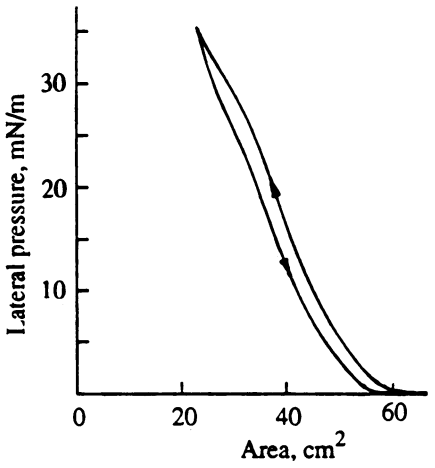

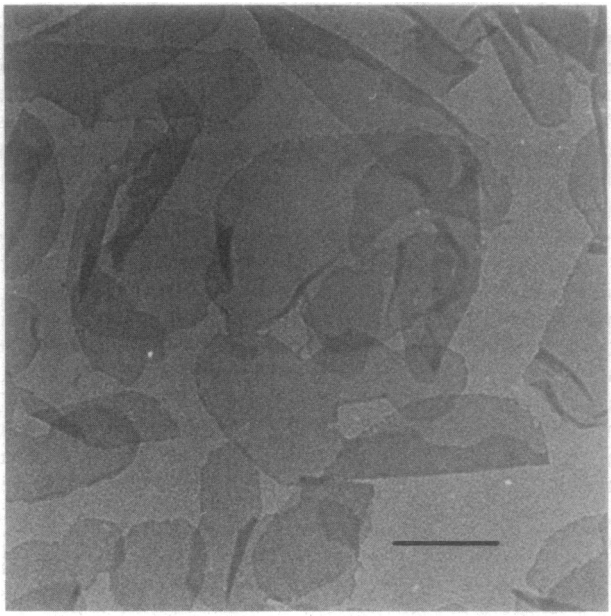

FIG. 2. (*Upper*) Pressure/area diagram after spreading purple membrane, indicating that the purple membrane stays at the air–water interface. (*Lower*) TEM micrograph of purple membrane, transferred from the air–water interface at a lateral pressure of 20 mN/m, showing homogeneous coverage. (Bar = 0.5 μm.)

before they were removed from the trough and "washed" with distilled water. After blotting most of the liquid with filter paper, the samples were air-dried. A typical TEM image of such a preparation showing the uniform coverage with purple membrane is presented in Fig. 2 *Lower*.

Some purple membrane preparations were finally coated at room temperature with Pt/C by electron beam evaporation in vacuum (5×10^{-6} mbar; 1 bar = 100 kPa). The nominal film thickness was ≈1.7 nm, according to the quartz crystal monitor reading.

HPI Layer Preparation. HPI layer sheets were isolated as described (11). A droplet of the aqueous HPI layer suspension was applied to freshly cleaved mica sheets or, alternatively, to Pt/C- or C-coated mica pieces or coverslips rendered hydrophilic by glow discharge in air at a pressure of ≈0.1 mbar. After a 10-sec adsorption period, excess water was blotted, and the preparation was washed once with distilled water before being air-dried. This preparation protocol results in nonhomogeneous coverage of the specimen support with local piling of HPI layer sheets.

Most of the HPI preparations were coated with Pt/C as described for purple membrane. For comparison we used

freeze-dried preparations coated with platinum/iridium/carbon (Pt/Ir/C) (21) of a nominal film thickness of 1.0 nm.

RESULTS AND DISCUSSION

Gold (100) Surface and *z* Calibration of the STM. Calibration of an STM means the determination of the relationship between *xyz* shifts of its tunneling tip and the voltage applied to its piezoelectric actuators. For *xy* calibration, a lattice of highly oriented pyrolytic graphite was used as a standard. In a tripod STM, the *x*, *y*, and *z* movements are driven by separate piezoelectric elements of the same type; *z* calibration does not pose a particular problem, since the results of the *xy* calibration can also be used for the *z* direction. For a single tube scanner, however, the *z* direction must be calibrated independently.

To use the atomic steps on a crystalline gold surface (prepared as described above) for *z* calibration, one must identify the crystallographic orientation of the surface being observed. Essentially, one must be able to distinguish between surfaces of Miller indices (100), (110), and (111).

Fig. 1 shows a typical picture of our gold preparation with large terraces and atomic steps. This picture was taken 9 days after the annealing; after 21 days, the monosteps and terraces could still be imaged, but there were many contamination dots on the terraces and the images appeared quite "noisy." Unfortunately, it is difficult to measure the apparent lattice constant (see Fig. 1 *Inset*), since the atomic corrugation of the surface is small (≈0.03 nm) and very often the periodicity is obscured by noise—probably due to contamination in air.

The distinction between the different crystal faces can also be made by their monostep heights $a/2$ for (100), $a/\sqrt{2}$ for (110), and $a/\sqrt{3}$ for (111) surfaces. The (100) and (111) step heights are fairly close to each other (0.204 and 0.236 nm). However, (111) terraces appear triangular in shape, whereas (100) and (110) are rectangular. We conveniently found that the (100) surface was the predominant one in our preparations. Since the (110) steps are >40% larger than the (100) steps, they are easy to discriminate, given the 10% accuracy in our height measurements.

To increase the accuracy of this calibration we took averages from >50 single and double steps. The rms deviation of the measured step heights was 0.02 nm.

To test the described calibration independently, we used a plain Pt/C-coated coverglass as a specimen, tilted it mechanically, and measured the corresponding effective tilt angle in the STM signal. According to the gold calibration, we obtained a tilt angle of 2.4° instead of 2.6°, as determined by the mechanical adjustments. Considering the estimated accuracy of 10% for the mechanical tilting, this macroscopic test confirms the *z* calibration by means of gold atomic steps.

Thickness Measurements on Purple Membrane. Fig. 3 *Upper* shows a typical STM image of a Pt/C-coated preparation of purple membrane. The periodicity of the membrane is not visible. The surface appears smooth apart from the short-range granularity of the coating film. The size of the grains ranges from ≈2 to 4 nm in width and the measured rms corrugation is ≈0.3 nm (see also ref. 13). To remove the influence of the granularity of the coating film, one must take averages over selected areas of the purple membrane as well as of the adjacent substrate devoid of purple membrane. Since the average thickness of the coating film can be assumed to be the same on both surfaces, the difference in height can be taken as a measure of the thickness of the purple membrane. For tilted samples, one must first remove the height ramp in the pictures before averaging. The thickness of the air-dried Pt/C-coated purple membrane was found to be 4.3 nm with a rms deviation of 0.1 nm.

We also measured the thickness of an uncoated preparation, as shown in Fig. 3 *Lower*. To obtain such images, it was necessary to resort to rather high tunneling voltages (>6 V) and very small tunneling currents (<0.5 pA). The humidity of the ambient air was not as critical as for imaging the uncoated HPI layer (22). The best images were obtained at a humidity of ≈60%. The apparent thickness values measured were smaller than for Pt/C-coated preparations and varied from one experiment to another; typical values were between 2.0 and 3.5 nm.

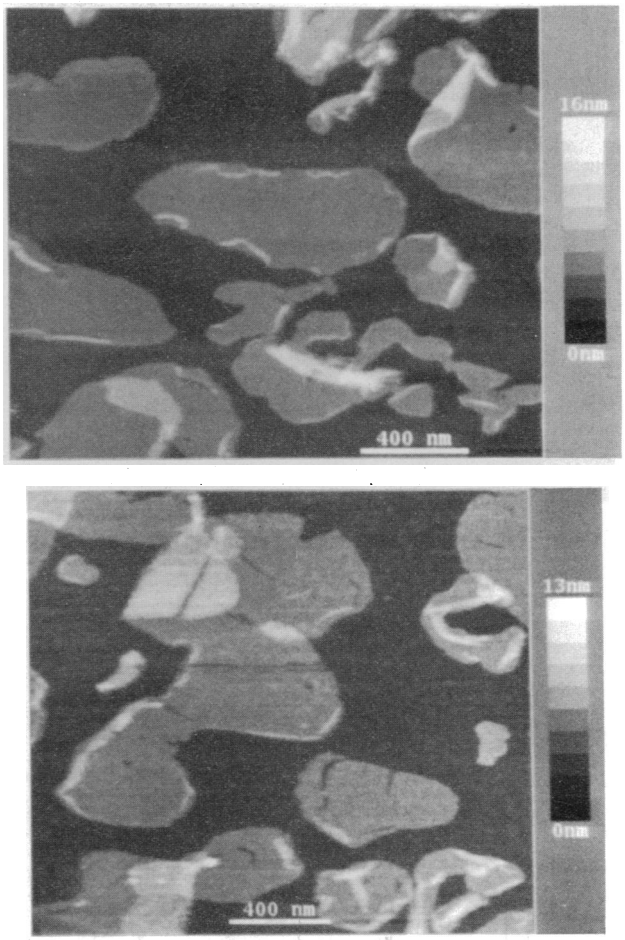

FIG. 3. STM images of purple membrane prepared by the spreading technique on Pt/C-coated mica. (*Upper*) Unprocessed STM image of a Pt/C-coated sample. Tunneling parameters: $U_{tip} = -1.0$ V; $I_t = 20$ pA. (*Lower*) STM image of an uncoated sample, image slightly processed by subtraction of ramps. Tunneling parameters: $U_{tip} = -12$ V; $I_t = 0.2$ pA; relative humidity = 60%. Similar pictures were also achieved with reversed polarity of U_{tip}.

Thickness Measurements on the HPI Layer. Fig. 4 *Upper* shows a typical STM image of an air-dried Pt/C-coated HPI layer. One can clearly see the periodic structure of the layer with pores at the center of the hexameric cores and indications of the spokes interconnecting the cores in some local areas. There is a substantial variation from one unit cell of the two-dimensional crystal to another. This is clearly visible in Fig. 4 *Lower*, where four line scans along one of the lattice base vectors are displayed. These line scans are aligned according to the core positions and include the step from the HPI layer to the support. The inter-unit-cell variations can be ascribed only partly to the roughness of the coating film. Most likely the adverse effects of specimen preparation on the protein (see below) affect it in a nonuniform manner, giving rise to an additional structural heterogeneity.

For the highly corrugated structure of the HPI layer, the averaging method must be modified for thickness measurements. Only the highest elevations of the structure define its

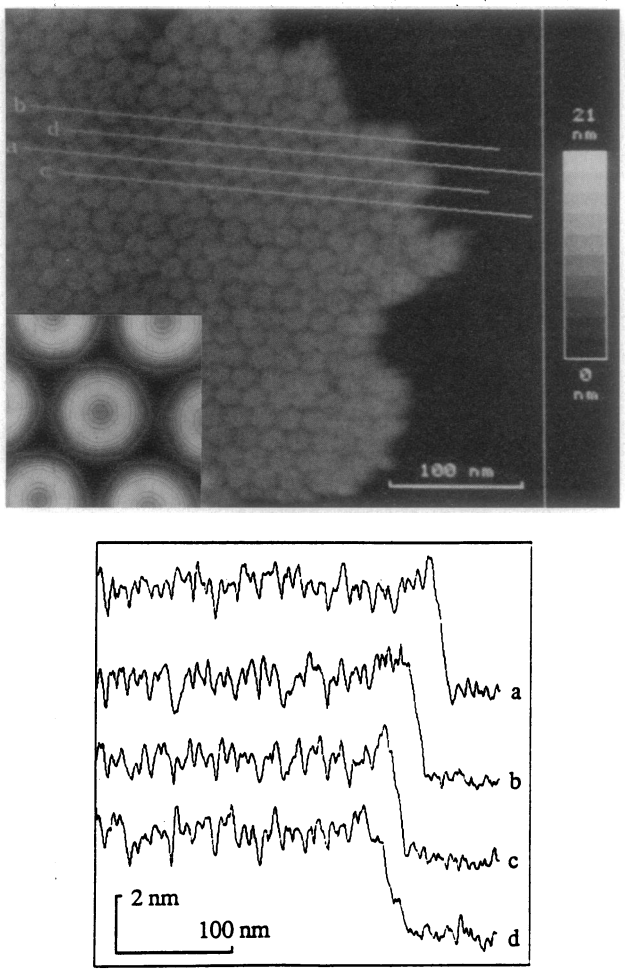

FIG. 4. (*Upper*) Typical unprocessed STM image of air-dried Pt/C-coated HPI layer on Pt/C-coated mica. Tunneling parameters: $U_{tip} = -1.0$ V; $I_t = 20$ pA. (*Inset*) Magnified motif average (size 32 nm × 32 nm) of this image with contour lines at 0.1-nm height intervals (total height range = 1.65 nm). (*Lower*) Cross sections along lattice lines as indicated. They include the step from the layer to the substrate. The line scans are aligned according to the core positions of the HPI layer. They clearly show the structure variation of the unit cells.

height. Since the HPI layer is a two-dimensional crystal layer and hence each unit cell is basically identical, it is sufficient to add up all available unit cells after properly aligning them and to search for the highest point in this motif average. Averaging techniques based on cross-correlation, which automatically provide partial compensation for geometrical distortions of the lattice, are well established in conventional TEM (23). Fig. 4 *Upper Inset* shows the motif average of the HPI layer imaged in Fig. 4 *Upper*. It is symmetrized according to its known *p*6 symmetry. The measured difference between maximum height in the motif average and substrate average is taken as the thickness of the HPI layer. Such data are listed in Table 1 for various sample preparation techniques and for the two possible orientations of the layer with respect to the substrate. The results will be discussed below.

Not included in Table 1 are the data from the uncoated HPI layer that was imaged under extreme conditions similar to those applied to the naked purple membrane. For successful imaging it was critical to keep the relative humidity >30%. The measured height turned out to be ≈4 nm (22).

Discussion of Errors in the Thickness Measurements. In discussing the accuracy and reliability of the height measurements, one must address the following problems that we consider to be particularly important: (*i*) In coated preparations the coating film is not structureless but has an intrinsic structure. (*ii*) With uncoated preparations the underlying imaging mechanism is not properly understood. (*iii*) The specimen may be deformed elastically during imaging because of the forces between sample and tip. (*iv*) In all preparations the structure of the biological macromolecule may change in the course of the preparation procedure.

(*i*) When averaging over flat specimen areas coated by a statistically granular film one can obtain a very accurate measurement of the mean level, provided the averaged area is large enough. With an average grain size of 3 nm and a height signal with a rms deviation of 0.3 nm, one needs a minimum area of ≈10 nm × 10 nm to obtain a rms deviation of 0.1 nm in the height average. In general it poses no problem to find even much larger areas in the STM images.

To obtain an estimate of the accuracy of the height level of the highest elevations of a corrugated structure like the HPI layer, one can take the rms deviation of the coating structure divided by the square root of the number of motifs averaged. Therefore, ≈10 motifs should be sufficient for an accuracy of 0.1 nm. This calculation was tested by applying the motif-averaging procedure to the substrate, treating it as if it were periodic. The remaining absolute variation in these motif averages of the substrate was always <0.1 nm for averaging of 50 and more motifs.

These considerations hold as long as the granularity of the coating film is only statistical. A deviation from a statistical distribution, however, can be caused by topochemical effects (local attraction or repulsion of Pt/C clusters by the surface topochemistry of the object), effects known as decoration in conventional electron microscopy (24, 25). On a periodic specimen, decoration will reflect the underlying periodicity. No periodic signal was observable in the evaluated purple membrane images, however.

For a corrugated structure like the HPI layer, decoration effects cannot be excluded that simply. However, it is known from experiments with Pt/C coating under conditions favoring decoration (26) that for the HPI layer the effects are small. Thus, for the two objects investigated here, decoration can be neglected.

(*ii*) For specimens with good surface conductivity such as Pt/C-coated samples, the STM will image the profile of the surface. For uncoated biological specimens, surface and bulk

Table 1. STM measurements of the thickness of HPI layer in metal-coated preparations

Sample support	Drying method	Outer surface up			Inner surface up		
		Height, nm	SD, nm	*N*	Height, nm	SD, nm	*N*
Mica/2 nm of Pt/C:GD	Freeze-dried	5.11	0.51	8	4.78	0.36	6
Mica/18 nm of C:GD	Air-dried	4.42	0.03	3	4.60	0.12	3
Mica/1.7 nm of Pt/C	Air-dried	4.32	0.22	8	4.33	0.14	5
Mica/1.7 nm of Pt/C:GD	Air-dried	3.82	0.21	7	4.16	0.20	5
Mica:GD	Air-dried	3.71	0.17	14	3.94	0.12	7

SD, root mean square deviation; *N*, number of measurements; GD, glow discharged. All air-dried samples were finally coated with 1.7 nm of Pt/C; the freeze-dried samples were coated with 1 nm of Pt/Ir/C. Measurements of uncoated hydrated HPI layer on Pt/C-coated coverslips result in a thickness of ≈4 nm.

conductivity are poor. A voltage drop across the specimen or tunneling into the specimen or even through it may occur. In these cases the tip will no longer follow the surface profile. In addition, the effective barrier height may change across the object giving rise to artifacts in the observed relief. The trustworthiness of thickness measurements on uncoated objects critically depends on a good understanding of the underlying imaging and conduction mechanism. For the images of the HPI layer in ref. 22, we assume sufficient conductivity for actually imaging the surface of the object. This is indicated by its similarity with the images of coated preparations and the reasonable agreement of measured thicknesses. In contrast, the measured thickness of the uncoated purple membrane is significantly smaller than the values obtained with coated preparations. So far we are unable to explain this difference. Further insights into the conduction mechanisms involved are needed to interpret the measured signals and possibly to deduce the correct thickness from them.

(*iii*) Since we have no direct evidence for elastic deformation of the specimens investigated, we will not discuss this problem further in this communication.

(*iv*) The object investigated by STM may change its thickness in the course of the preparation. There are two major factors to consider: forces acting during adsorption onto the substrate and effects of surface tension and of dehydration during air or vacuum drying. The more open and flexible a structure is, the more prone it is to distortion; in unfavorable cases the result may be (partial) collapse and substantial flattening. The effects may differ depending on the orientation of the specimen, as found in TEM investigations (6, 27).

Adsorption forces and drying effects are probably also responsible for the observed variation among the unit cells of the HPI layer (see Fig. 4 *Lower*). A variation in position of the highest elevations in the individual units results in a further decrease of height in the motif averages and with it in the measured thickness of the specimen.

Therefore, it is important to minimize all these effects by appropriate preparation techniques. For example, freeze-drying prior to coating eliminates the worst surface tension effects, as indicated by the higher resolution in the motif averages. Therefore, it is not surprising that this preparation also gives the highest thickness values (Table 1). The thickness of $\approx$5 nm is in reasonable agreement with 6.5 nm as obtained in three-dimensional reconstructions from TEM tilt series of HPI layer embedded in negative stain (27). Thickness measurements by other methods range from 6.9 to 8.6 nm (6), as mentioned before.

In the STM experiments, differences in height are found, depending on the orientation of the HPI layer with respect to the support. A greater height is measured with freeze-dried preparations when the more hydrophobic and relatively rigid inner surface interacts with the support. The outer surface contains more flexible segments of the polypeptide chain and hence is more liable to distortion. These effects are obscured with preparation methods that lead to substantial flattening anyway (i.e., with all air-dried preparations).

Air-dried samples prepared on various substrates showed the influence of the substrate. The lowest measured thicknesses (3.7 nm) were found for deposition on a freshly cleaved and plasma-cleaned mica surface. In comparison with an evaporated carbon film, the mica must be regarded as the more reactive surface. Again, when comparing mica supports coated with Pt/C, those rendered reactive by glow discharge in air give significantly lower average thicknesses than the untreated ones. Glow discharge promotes the adsorption of the HPI layer, as reflected by much denser coverage with adsorbed sample. This can be taken as evidence for the enhanced reactivity of the support, which, with this specific sample, entails some flattening.

In contrast to the HPI layer, purple membrane does not seem to be liable to flattening effects, probably because of its densely packed structure. The thickness measured for the air-dried and Pt/C-coated purple membrane is very close to the value known from x-ray experiments (10).

In conclusion, one can say that the STM is a very useful tool for measuring the thickness of biological objects. It provides the height signal directly. The trustworthiness of the results strongly depends on the rigidity of the object and on its conductivity. Poor conductivity can be overcome by metal coating, which lowers the resolution, however. A major problem with many specimens is the deformation of the object during adsorption onto the substrate and during drying. Our measurements show clearly that the choice of the support may be a critical factor in thickness measurements.

The STM with the tripod scanner was kindly made available to us by Prof. Dr. R. J. Behm (Munich). We thank Dr. M. Amrein (Zurich) for providing us with preparations of freeze-dried Pt/Ir/C-coated HPI layer, Mrs. S. Messen (Martinsried) for providing us with purple membrane, and Dr. B. M. Phipps (Martinsried) for critically reading the manuscript. The work was supported by the Deutsche Forschungsgemeinschaft (SFB-266-B4).

1. Baldwin, J. M., Henderson, R., Beckman, E. & Zemlin, F. (1988) *J. Mol. Biol.* **202,** 585–591.
2. Kühlbrandt, W. & Downing, K. H. (1989) *J. Mol. Biol.* **207,** 823–828.
3. Jap, B. K. (1989) *J. Mol. Biol.* **205,** 407–419.
4. Sass, H. J., Büldt, G., Beckmann, E., Zemlin, F., van Heel, M., Zeitler, E., Rosenbusch, J. P., Dorset, D. L. & Massalski, A. (1989) *J. Mol. Biol.* **209,** 171–175.
5. Rachel, R., Jakubowski, U., Tietz, H., Hegerl, R. & Baumeister, W. (1986) *Ultramicroscopy* **20,** 305–316.
6. Wildhaber, I., Gross, H., Engel, A. & Baumeister, W. (1985) *Ultramicroscopy* **16,** 411–422.
7. Jésior, J.-C. & Wade, R. H. (1987) *Ultramicroscopy* **21,** 313–320.
8. Oesterhelt, D. & Stoeckenius, W. (1971) *Nature (London) New Biol.* **233,** 149–152.
9. Henderson, R. & Unwin, P. N. T. (1975) *Nature (London)* **257,** 28–32.
10. Henderson, R. (1975) *J. Mol. Biol.* **93,** 123–138.
11. Baumeister, W., Karrenberg, F., Rachel, R., Engel, A., Ten Heggeler, B. & Saxton, W. O. (1982) *Eur. J. Biochem.* **125,** 535–544.
12. Besocke, K. (1987) *Surf. Sci.* **181,** 145–153.
13. Guckenberger, R., Kösslinger, C., Gatz, R., Breu, H., Levai, N. & Baumeister, W. (1988) *Ultramicroscopy* **25,** 111–122.
14. Hallmark, V. M., Chiang, S., Rabolt, J. F., Swalen, J. D. & Wilson, R. J. (1987) *Phys. Rev. Lett.* **59,** 2879–2882.
15. Schneir, J., Sonnenfeld, R., Marti, O. & Hansma, P. K. (1988) *J. Appl. Phys.* **63,** 717–721.
16. Wiechers, J., Twomey, T., Kolb, D. M. & Behm, R. J. (1988) *J. Electroanal. Chem.* **248,** 451–460.
17. Oesterhelt, D. & Stoeckenius, W. (1974) *Methods Enzymol.* **31,** 667–678.
18. Trurnit, H. J. (1960) *J. Colloid Sci.* **15,** 1–13.
19. Weast, R. C., ed. (1988) *CRC Handbook of Chemistry and Physics* (CRC, Boca Raton, FL), 69th Ed., F-33.
20. Langmuir, I. & Schaefer, V. J. (1938) *J. Am. Chem. Soc.* **60,** 1351–1360.
21. Amrein, M., Stasiak, A., Gross, H., Stoll, E. & Travaglini, G. (1988) *Science* **240,** 514–516.
22. Guckenberger, R., Wiegräbe, W., Hillebrand, A., Hartmann, T., Wang, Z. & Baumeister, W. (1989) *Ultramicroscopy* **31,** 327–332.
23. Saxton, W. O. & Baumeister, W. (1982) *J. Microsc. (Oxford)* **127,** 127–138.
24. Baumeister, W., Guckenberger, R., Engelhardt, H. & Woodcock, C. L. F. (1986) *Ann. N.Y. Acad. Sci.* **483,** 57–76.
25. Bachmann, L., Weinkauf, S., Baumeister, W., Wildhaber, I. & Bacher, A. (1989) *J. Mol. Biol.* **207,** 575–584.
26. Winkler, H., Wildhaber, I. & Gross, H. (1985) *Ultramicroscopy* **16,** 331–339.
27. Baumeister, W., Barth, M., Hegerl, R., Guckenberger, R., Hahn, M. & Saxton, W. O. (1986) *J. Mol. Biol.* **187,** 241–253.